Nearest Neighbor Spacing of Fair Weather Cumulus Clouds

JOACHIM H. JOSEPH*,@ AND ROBERT F. CAHALAN*

** Laboratory for Atmospheres, Goddard Space Flight Center, Greenbelt, Maryland*
@ Dept. of Geophysics and Planetary Sciences, Beverly and Raymond Sackler Faculty of Exact Sciences, Tel Aviv University, Ramat—Aviv, Israel

(Manuscript received 7 November 1988, in final form 6 March 1990)

ABSTRACT

Histograms of nearest neighbor spacings of fair weather cumulus at 15 locations over the world's oceans are presented based on the analysis of high resolution LANDSAT 3 Multispectral Scanner images for amounts of cloud cover ranging from 0.6% to 37.6%. These histograms are found to be essentially the same at all locations analysed, similarly to our previous findings on the size distributions and the fractal dimensions of the perimeters for this cloud type.

The nearest neighbor spacings are linearly dependent on the effective cloud radii, with a proportionality factor ranging from five to twenty. The histograms peak at about 0.5 km. Nearest-neighbor spacings smaller than about a kilometer, associated with cumulus clouds with an effective radius less than a few hundred meters, have a distribution of cloud centers that is almost independently distributed in the horizontal plane and show a tendency for the formation of clumps. Larger spacings of up to thirty kilometers occur and are associated with the larger clouds. These latter spacings are not independent.

1. Introduction

The present paper deals with several aspects of the geometrical properties of the fair weather cumulus cloud field. The reasons for investigating such topics are several. First, this type of persistent convective cloud covers a large fraction of the globe at any particular time, especially in the low latitudes and in the midlatitudes in summer (e.g., Cahalan et al. 1982; Hahn et al. 1984). Second, the proper treatment of shallow moist convection and its ensuing cloudiness is important in modeling the global climate (Betts and Miller 1986). However, modeling of shallow cumulus convection and derivation of the cloud field organization under various atmospheric conditions is an ongoing and difficult problem and its parameterization for use in simulations is rudimentary. Several studies have been recently published in which attempts were made to model various mechanisms responsible for determining cumulus cloud field geometry and its development (e.g., Cho 1973; Fraedrich 1976, 1977; VanDelden and Oerlemans 1982, 1984; Bretherton 1987a,b). Third, many studies have shown the importance of cloud geometry in the radiative transfer of energy through cloud fields (e.g., Paltridge 1974a,b); Stephens 1976; Davies 1978; Gube and Schmetz 1980; Welch et al. 1980; Harshvardan and Thomas 1984; Joseph 1985; Welch and Wielicki 1985; Joseph and Kagan 1988; Cahalan 1989). Last, the experimentally determined values of many remotely sensed atmospheric and surface parameters must be appropriately corrected for the effect of clouds before using them in models and in prediction algorithms (Kaufman 1987).

Evidence of the inhomogenuous structure of even stratus clouds is steadily accumulating (e.g., Baker and Latham 1979; Derr and Gunter 1982; Cahalan and Joseph 1989; Cahalan and Snider 1989). The geometrical structure of cloud fields has been but infrequently studied with very high resolution in the past. Some studies are based on airplane (e.g., Blackmer and Serebreny 1962; Plank 1969; Hozumi et al. 1982)—others on satellite data (e.g., Gifford and McKee 1977; Lovejoy 1982; Wielicki and Welch 1986; Cahalan and Joseph 1989). Plank's study was the first detailed analysis of cumulus cloud fields obtained using aircraft and involved visual examination of U-2 photographs over the Florida area. Plank produced frequency distributions of equivalent cloud diameter $[2\sqrt{(\text{area}/\pi)}]$, minimum and maximum equivalent diameter, cloud cover, cloud volume and aspect ratio—all as a function of time of day. One important result of his analysis was that the size distribution peaks at the smallest radii in the image. A second is that the aspect ratio of nonraining fair weather cumulus clouds in the Florida area is approximately one from morning till about midaf-

Corresponding author address: Dr. Joachim H. Joseph, Dept. of Geophysics and Planetary Sciences, Beverly and Raymond Sackler Faculty of Exact Sciences, Tel Aviv University, Ramat—Aviv, Tel Aviv 69978 Israel.

ternoon, independently of cloud cover or maximum cloud areas, so that the observed area of a single such cloud is representative also of its thickness.

Some results on the fractal properties of clouds relevant to the present study were published in a previous paper (Cahalan and Joseph 1989). The aspects pertaining to cumulus clouds are summarized here, for convenience.

First, the histogram of cloud sizes in terms of equivalent radii [$r_e = (\text{area}/\pi)^{0.5}$] is best fitted by a bimodal power law, $Kr^{-\beta}$. The average cross-over radius from one mode or power to another, r_{break}, is at about 0.5 $\pm$ 0.3 km. The values of the powers for cumulus clouds are 2.8 $\pm$ 0.3 for the small clouds and 3.7 $\pm$ 1.2 for the large ones. Second, two fractal dimensions of the perimeters are needed to describe the [log(perimeter), log(area)] relationships—1.27 $\pm$ 0.03—for the smaller clouds and 1.55 $\pm$ 0.06 for the larger ones of more complex shape. The radius of transition from one fractal dimension to the other is always very close to that at which the break in the size distribution occurs. Third, the smaller and smoother clouds have one center of brightness; the clouds that are larger and of more complex shape have at least two and usually more than three. Fair weather cumulus clouds thus seem to fall into two distinct classes, each presumably with its own physical formation mechanism—"small" and "large" clouds. If, for example, the smaller, smoother ones with the lower power of the size distribution and lower fractal dimension are in fact formed in the boundary layer by Gaussian fluctuations of a scalar field above a lifting condensation level, the fractal dimension of the perimeters should be close to 4/3 (Lovejoy 1982; Mandelbrot 1984; Hentschel and Proccaccia 1984). The actual value that we find for the fractal dimension of the "small" clouds is close to that value as shown in our previous paper. Second, let us recall that the aspect ratio of nonraining FWC clouds is one (e.g., Plank 1969). The horizontal effective radius of the clouds is therefore equal to one-half of their thickness. For the "small clouds," this thickness must be less than or comparable to the depth of the boundary layer. The depth of the boundary layer in which the small clouds form is therefore likely to be the natural upper bound on their thickness or radius and thus might be responsible for the breaks in the slopes of our experimental histograms.

The larger clouds with the more complex shapes may be formed by several different physical phenomena. One may have random merging (e.g., Simpson et al. 1980), or clumping (Randall and Huffman 1980); other mechanisms involve organization into planforms due to either local phenomena related to shallow cumulus convection (VanDelden and Oerlemans 1984; Bretherton 1984, 1987a,b) or to nonlinear interactions via gravity waves with the free atmosphere above the boundary layer (Clark et al. 1986). From the above the importance of the acquisition of more data, global in scope, on the organisation of cloud fields is obvious. High resolution LANDSAT images are an almost ideal means for this purpose. The aim of this study therefore is to continue the description of the morphological properties of cloud fields derived from high resolution LANDSAT imagery begun in our previous paper, focusing now on the spacing of fair weather cumulus.

Both radiative and dynamic interactions between clouds depend upon intercloud spacing. Consider an evolving cloud moving in and with a cloud field. It will be influenced in its development by the general meteorological conditions in the ambient atmosphere. Second, it will experience the combined effects of all other clouds, both past and present—due to radiative interactions with other clouds, due to the spatial variability in the availability of water vapor associated with the previous existence of clouds, and due to dynamic organization of the intercloud distances, for example, by the excitation of gravity waves (Clark et al. 1986). These effects may be divided, for the present purposes, into two parts for each individual cloud—an integrated systematic effect due to the smoothed or average effect of all clouds in the field and the effect of the clouds in its immediate neighborhood. The first part will not change much either from cloud to cloud or in time for a given cloud under statistically homogenuous conditions. The second part, on the other hand will differ from cloud to cloud as well as change in time unless the field is in a homogenuous steady state (e.g., Bretherton 1987a,b). Therefore, the number, locations and sizes of close neighbors to a cloud will be different for each cloud in the field and will also change in time for each cloud. The simplest possible measure for the interaction distance of two clouds is the average distance between cloud centers. Clouds much closer to one another than the average distance will interact more strongly. In order to get an initial idea on the probability of cloud–cloud interaction—or on the "lebensraum" or living space of a cloud—we decided to derive the nearest neighbor spacing histograms and associated distributions. Alternative measures of cloud–cloud interaction include: the up- and/or downdraft area of each cloud if definable from the data, the area around a cloud in which one finds less than a certain percentage of the areas of neighboring clouds, and some separation scale or correlation length if apparent in the image. All these alternatives to the nearest neighbor spacing are problematic in some way, either because of their relevance or applicability to the problem or because of the difficulty of their proper definition from the data. The nearest neighbor spacing histogram, in addition, is readily tested for the occurrence of independently distributed random spacings (Chandrasekhar 1943) which is one of the purposes of the present analysis.

The LANDSATs were chosen for this analysis because they are one of the few commercially available sources of high resolution digital cloud data. They have the advantage of a wider field of view than aircraft, so

that results are representative of areas resolvable by current general circulation models. However, at the same time the practical resolution of the LANDSAT data for cloud area, about four pixels (Cahalan and Joseph 1989), approaches that of typical aircraft measurements. This provides an important link between the complex phenomena seen in real clouds on all size scales and the low resolution, largely theoretical, parameterization of clouds in models of the atmosphere. Thus, though the LANDSAT data are extremely voluminous, even for a single scene, and are expensive to analyze (see section 2), one is compensated by the uniquely high resolution view of the horizontal structure of cloud fields. A disadvantage of the LANDSAT data is that they are available only at one time—mid morning about 0930 LST. Thus, in order to study variation in time of cloud properties, they need to be supplemented by other similar remotely sensed information.

In section 2 we describe the properties of the LANDSAT 3 and of its Multispectral Scanner [MSS] instrument as well as the various problems encountered and methods used in analysing the imagery obtained from it. In section 3 we present the distribution of nearest neighbor spacings (henceforth n.n.s.). In section 4, we present the experimental relationship between cloud effective radius and nearest neighbor spacing. Finally, in section 5, we discuss and summarize our results.

2. Analysis of LANDSAT MSS images

The MSS instrument on LANDSAT 3 has four bands: the yellow band (MSS 4, 0.5–0.6 μm), the red band (MSS 5, 0.6–0.7 μm), and two near-infrared bands (MSS 6, 0.7–0.8 μm and MSS 7, 0.8–1.1 μm). Each MSS scene has an area of 185×170 km^2, with the short axis oriented parallel to the satellite track. The sun-synchronous near-polar orbit is at an altitude of about 920 km with a nominal 0930 LST equatorial crossing time. The orbit repeat cycle is 18 days, so that each area is directly underneath the satellite orbit only once every 18 days.

Each pixel has a range of 0 to 63 in digital counts, which in processing is converted to a linear range of 128 levels of brightness. The MSS gain on LANDSAT is optimized for the observation of land surface properties, so that clouds are often saturated in brightness, in particular for high gain images. The maximal possible radiance that can be measured corresponds to that of a Lambertian grey reflector with an albedo of 50 percent for a solar zenith angle of 45 degrees. After geometrical corrections, each pixel corresponds to an area of 57×57 m^2 or 0.003249 km^2, so that there are close to ten million pixels per spectral band in each image, or about forty megabytes per image.

The images are available to us digitally in the form of one 6250 bpi tape per scene, including all spectral bands, as well as in the form of black and white prints of selected bands. After reading, copying and checking the quality of the tapes, we identify from the black and white prints the general location of the cloudy and clear areas not to be analyzed because of either poor data quality or unsuitable background. A list of the images analyzed, their locations, coordinates and dates of acquisition are given in Table 1. The cumulus cloud field images used in this study are similar in general appearance and properties to those analyzed and shown in previous publications (e.g., Wielicki and Welch 1986).

The data storage and analysis problems are formidable. At ten megabytes per image and per band, the analysis of two bands for each of the 15 images represents a total data volume of about 300 megabytes. An additional 300 megabytes have been analyzed and then could not be used due to insufficient cloud cover, inhomogenuous backgrounds or low data quality.

One of the central problems in the current project is the discrimination between clear and cloudy pixels. The difficulties of determining an appropriate threshold

TABLE 1a. Image IDs, coordinates, locations and times of acquisition.

Case	Image ID	Center coordinates	Location	Path-row	Year/day
7013	22555-07291	N31°46′ E34°11′	Israel	188-038	76/212
7024	22072-15003	N23°04′ W78°44′	Bahamas	014-044	80/268
7025	22073-15055	N24°30′ W79°47′	Florida	015-043	80/269
7026	22056-15113	N24°30′ W81°11′	Florida	016-043	80/252
7028	22109-15054	N24°30′ W79°47′	Florida	015-043	80/305
7029	22127-15052	N24°28′ W79°40′	Florida	015-043	80/323
7030	30277-01144	N27°20′ E129°7′	Okinawa		78/341
7032	30346-21395	N15°50′ W179°20′	Marshalls	083-049	79/045
7033	30369-18510	S15°51′ W142°21′	Toamotus	052-071	79/068
7034	30364-11203	N14°24′ W24°25′	Cape Verde	226-050	79/063
7035	30364-11201	N15°50′ W24°24′	Cape Verde	226-049	79/063
7064	22038-15094	N30°14′ W79°35′	Florida	016-039	80/234
7066	22312-15310	N28°46′ W85°39′	Gulf Mexico	020-404	81/142
7067	30661-15303	N28°46′ W85°39′	Gulf Mexico	020-040	79/360
7072	31565-15595	N28°46′ W91°25′	Gulf Mexico	024-040	80/168

TABLE 1b. Parts of images not analyzed and reasons. Line numbers and column numbers in one column constitute a set. Reasons: A—Land or shallow ocean; B—Haze; C—Data missing or in error.

Case: 7013: Reasons not analyzed: Land and/or shallow ocean					
Lines	1–700	701–1200	1201–1500	1501–2100	2101–2983
Columns	900–3548	1200–3548	1600–3548	1900–3548	1–3548
Case: 7025: Reasons not analyzed; Land and/or shallow ocean					
Lines	1–2000	1–2983	2100–2983		
Columns	1–950	2650–3548	750–2200		
Case 7026: Reasons not analyzed: Land and/or shallow ocean					
Lines	1–1800				
Columns	1–1200				
Case: 7028: Reasons not analyzed: Land and/or shallow ocean					
Lines	1–1200	1–2983	2100–2983		
Columns	1–950	2650–3548	750–2200		
Case 7029: Reasons not analyzed: Land and/or shallow ocean					
Lines	1–1200	1–1500	1501–2983	2100–2983	
Columns	1–700	2400–3548	2600–3548	500–2100	
Case: 7030: Reasons not analyzed: Land and/or shallow ocean					
Lines	1–219	407–749	1075–1277	1970–2340	
Columns	1245–1700	934–1330	544–950	1–650	
Case: 7033 A A C C					
Lines	1100–2250	2400–2679	880–930	2680–2800	
Columns	1520–2200	200–700	1–3548	1–3548	
Case: 7034: Reasons not analyzed: Land and/or shallow ocean					
Lines	450–700				
Columns	1500–1900				
Case: 7035 Haze Haze Land or shallow ocean					
Lines	2–1299	1300–2983	2640–2983	1980–2200	2420–2983
Columns	1–3548	2601–3548	1320–2200	1–200	2201–3548
Case: 7064: Reason—Haze					
Lines	660–1500	1760–2983			
Columns	2200–3548	140–3548			
Case: 7066: Reason—Haze					
Lines	1–1800				
Columns	1–3548				
Case: 7072 C B A					
Lines	1–2983	1–220	1–880		
Columns	1–1030	1320–1685	1686–3548		

to derive accurate cloud cover are well known (e.g., Wielicki and Welch 1986). In addition, we had a problem special to the use of LANDSAT 3 data, that is, that there is no independent means available to test the result of the analysis. In the case of LANDSAT 4 and 5, the thermal IR band is available to derive cloud cover by the spatial coherence method, and a brightness threshold may then be chosen in the bands located in the solar spectral range to reproduce the same cloud cover (Cahalan and Joseph 1989). The associated cloud base temperature threshold compares favorably with in situ measurements (Cahalan and Snider 1989). If that is not possible, ad hoc statistics or climatological assumptions have to be made (e.g., Welch and Wielicki 1986; Welch et al. 1988). We tried to develop for use with LANDSAT 3, a method that would not depend

on such ad hoc assumptions and could be tested against others using LANDSAT 3 as well as LANDSAT 4 and 5 data. We compared four different methods for the solar MSS bands of LANDSAT 3, 4 and 5 data. They include the TRM method (Welch and Wielicki 1985). Some of the results are shown in Table 2a (see also Joseph 1986, 1987; Cahalan and Joseph 1989). In addition we also tested a Laplacian edge definition technique (Joseph 1986) which turned out not to be useful for clouds.

The rationale behind the one that we decided to employ in the routine analysis, termed "bispectral iterative method" or BIM, may be summarized in the following way. It is usually difficult to define a threshold from a solar IR (MSS 7) or red band (MSS 6) alone using either intensity histograms or cloudiness because the cloudiness decreases monotonically with increasing threshold without any sharp jumps or discontinuities—e.g., see our Fig. 1b—and the histograms show no clear valleys or changes of slope (Welch and Wielicki 1986; Welch et al. 1988). The total number of clouds or the number of clouds below a certain size close to the limit of resolution do however show sharp changes even in the red and solar IR bands—see our Figs. 1a,b for a particular case. Second, even though the intensities of any given single pixel in the various LANDSAT 3 bands are nominally proportional, this is not necessarily so in practice for the very low intensities. However, this is exactly where we try to define a threshold in any given band. Our approach therefore is bispectral, based on both the cloudiness as well as on the number of clouds in each band. The lower limit of brightness for cloud pixels in each band is iteratively deduced by starting with a threshold close to the maximum cloud brightness and reducing it until the following conditions are met simultaneously:

1) the total cloudiness begins to rapidly climb to 100 percent;

TABLE 2a. Typical sample comparison of all methods developed for threshold determination and applied to LANDSAT 3 data [Case 7025] for detailed comparisons of all cases, see Joseph 1986).

	PCP (1)	BSH (2)	WW (3)	BIM (4)
MSS 4	55 ± 5	50 ± 2	57 ± 4	59 ± 2
MSS 7	2 ± 1	2 ± 2	2 ± 2	2 ± 2

(1) PCP: Probability of cloudy pixel. Calculation of probability of pixel being cloudy in each band based on set of assumptions on Gaussian shape of cloud and background histograms. Iterated between bands for final results.

(2) BSH: Bispectral histograms. Removal of average non-cloud background from bispectral histogram thru experimental determination of the latter in each case and band.

(3) WW (1986): Wielicki and Welch (1986). Single band determination of threshold based on ad-hoc assumptions.

(4) BIM: Bispectral iterative method. Method described in text and adopted for analysis.

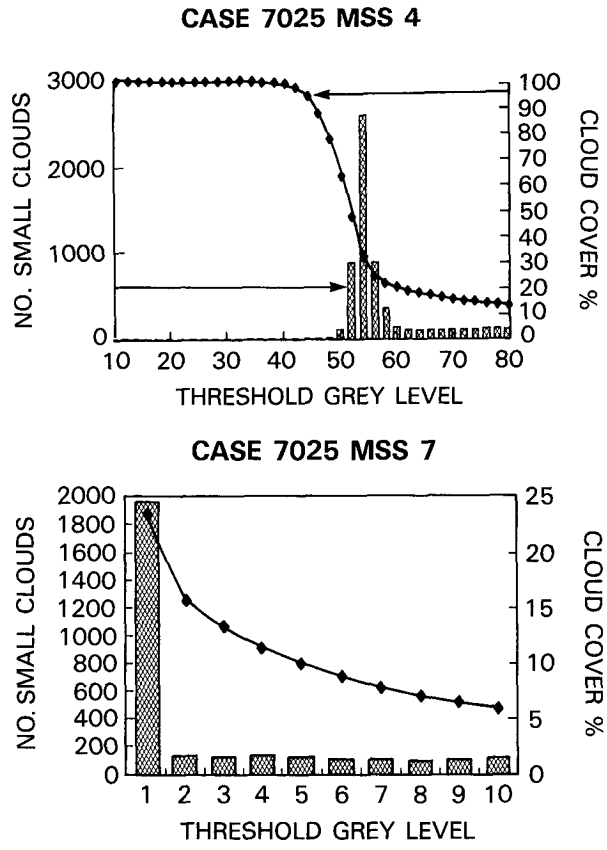

FIG. 1. (a) Determination of the threshold using the cloud cover and number of "small clouds" in band 4 of Case 7025. Threshold selected 59. (b) Determination of the threshold using the cloud cover and number of "small clouds" in band 7 of Case 7025. Threshold selected 2.

2) the number of "small" sub-resolution clouds (less than four pixels in area) starts to increase rapidly [viz. the noise level has been reached] and then drops to one—the whole scene becomes one "cloud."

We put the initial threshold in each band at one grey level above the point at which the strong increases start.

Then the results in the two bands used, MSS 4 and MSS 7 for LANDSAT 3, are intercompared and the thresholds are iteratively and simultaneously adjusted up or down by a few grey levels till the following conditions are fulfilled:

(i) the total degree of cloud cover in all bands is equal;

(ii) the total number of clouds is equal in all bands;

(iii) the locations of the cloud centers are identical in all bands and the cloud outlines overlap.

The final thresholds adopted are image-dependent and are given in Table 2b for all cases analyzed. To illustrate our method, Figs. 1a,b show the number of "noise clouds" (clouds of less than four pixels in area) versus threshold, and the percentage of cloud cover versus the

TABLE 2b. Location and thresholds for the LANDSAT 3 data. Based on the BIM technique; the other methods give very similar results.

Case	Location	Threshold Band 4	Threshold Band 7
7013	Mediterranean west of Israel	20	3
7024	Bahamas, Atlantic Ocean	21	3
7025	Straits of Florida	59	2
7026	Straits of Florida	21	3
7028	Straits of Florida	69	2
7029	Straits of Florida	65	2
7030	Okinawa, Pacific Ocean	43	3
7032	Marshall Islands, Pacific Ocean	82	7
7033	Tuamotu Islands, Pacific Ocean	77	6
7034	Cape Verde Islands, West Africa	77	6
7035	Cape Verde Islands, West Africa	81	7
7036	Cape Verde Islands, West Africa	77	6
7060	Bahamas Islands, Atlantic Ocean	22	3
7064	East of Florida, Atlantic Ocean	27	5
7066	Gulf of Mexico	24	5
7067	Gulf of Mexico	17	4
7072	Gulf of Mexico	43	10

threshold, and the percentage of cloud cover versus the grey level threshold in Bands 4 and 7, respectively. The threshold chosen in Band 4 (0.55 mm) is 59 and in Band 7 (1.0 μm) is 2. In both bands, the threshold is just before the precipitous rise in the number of small clouds as well as of that of the percentage of cloud cover with decreasing threshold intensity in Band 4 (see Fig. 1a) indicating that the noise level of the data has been reached. In Fig. 1a one can also see that soon after the noise level has been reached, the number of small clouds drops to zero because the whole scene becomes one large cloud. In the TRM method (Welch and Wielicki 1985), the threshold for cloud/no-cloud discrimination is put 3 percent above the peak intensity of the background. That particular, purely empirical value, of the threshold does give identical results to those obtained by our method in the present application—viz. cumulus clouds over the ocean. In general, such an empirical threshold will likely have to be determined separately for each type of cloud over each type of surface on the basis of accumulated statistics. Any improvement in the value of the threshold factor on the basis of new statistics might necessitate a reanalysis of all the previous results. In a previous paper (Cahalan and Joseph 1989), we show by direct application of our method to LANDSAT 4 and 5 data over sea, which include the thermal IR, that the degrees of cloud cover derived by both the Welch and Wielicki TRM and by our method are identical and compare equally well to the thermal IR results. We may take as a further confirmation of the utility of our method that in the a.m. paper, the size distribution parameters and the fractal dimensions of the perimeters derived from the LANDSAT 4 and 5 cloud data are found to be identical to those found from the LANDSAT 3 data under similar atmospheric conditions.

We would like to suggest the use of a multiband approach, like our own, also for earth observation satellites other than LANDSAT 3 even when other independent experimental or statistical data are available for calibration. It is just as good over sea as the other well-tested method (TRM) and just as easy to apply. In addition, it does not depend on any ad hoc assumption which may have to be changed from case to case and guarantees internally consistent, constraints on the results of the analysis. The only other way to verify the computer analysis as to the location, area, number and shape of the clouds in a spectral image would be by a laborious visual examination of the same image on a scanning microdensitometer. The application of any thresholding method over land is a difficult problem due to the spectral and spatial variation in the albedos and will be considered in a subsequent paper.

For the sake of brevity, we present the results of the analysis in this paper in terms of one band only, usually Band 4 (0.55 μm). We must therefore first illustrate the consistency of the results of the analysis in two bands, MSS4 and MSS7. In Table 3, we show for several parameters, the average over all cases of the ratio of the difference between the results in Bands 4 and 7 to the average of Bands 4 and 7. The averaged and normalized difference is never more than 3 percent. Consequently, the data in Table 3 indicate that once the thresholds are properly determined, one can safely study the results in one band only.

The next step is the construction of a binary map of "cloud" and "no-cloud" pixels and the definition of a group of cloud pixels as a contiguous cloud. A given pixel $x_{i,j}$ (in row i and column j) of a spectral image is "cloudy" if it has a grey level or brightness larger than the appropriate threshold value. Any contiguous pixel, sharing an edge or a vertex, with a given cloudy pixel is taken to be part of the same cloud.

TABLE 3. The average percentage difference between the results in two bands of the analysis for several parameters. The numbers shown are, for each parameter, the difference between the results from MSS Band 4 and Band 7 of LANDSAT 3, divided by the average of the two bands, and then averaged over the 15 available scenes. The values given are in percent.

Parameter	Percent difference
Cloud cover	1.5
K size distribution	3.1
b size distribution	−2.6
n Weibull distribution	−0.7
b Weibull distribution	−2.4
a Weibull distribution	−2.0

A running set of two lines is scanned simultaneously, so that during each scan, each interior pixel has four neighbors: its left neighbor on the same line and its three closest neighbors in the line above. Pixels on the left margin have two neighbors; those on a right margin have three. After each scan a set of clouds is defined and each is numbered. When the next line down is added to the set, the first line of the previous couple is dropped and a new scan is started. Some of the clouds in the database may then turn out to be connected through pixels in the new line. This leads to a renumbering of the clouds in the database as well as a recomputation of the total number of clouds and reorganization of the cloud number set, dropping "empty" clouds. This procedure is carried through till the bottom of the image is reached.

Cloud perimeters are determined for each cloud by adding the number of outside edges of pixels in the E–W direction, $X_k(i,j)$, times their length, Dx, to those in the N–S direction, $Y_k(i,j)$, times the latters' length, Dy. The kth cloud thus has a perimeter P_k given by

$$P_k = \sum_{i,j} [X_k(i,j)\Delta x + Y_k(i,j)\Delta y] \qquad (1)$$

where $X_k(i,j)$ is the number of east–west outside edges of pixels of cloud k in row i and column j, $Y_k(i,j)$ is the number of north–south outside edges of pixels of cloud k in row i and column j and the sums are over the relevant numbers of pixels for each cloud. All edges abutting noncloud areas, including holes, are counted. We do not take into account that both single perimeter pixels and "non-cloud" pixels abutting on cloud pixels may be partially cloudy. The determination of possible partial cloudiness of single cloud or other pixels is impossible except by assumption, e.g., 50 percent coverage. The assumption of 50 percent cloud cover for perimeter pixels does not increase accuracy and may lead to an underestimate of both perimeter and area in particular for smaller clouds. On the other hand, the fact that we do not smooth the serrated edges of our clouds leads to a possible overestimate of perimeter and area of about the same magnitude. As we have shown in a previous section that the choice of the threshold between cloud and noncloud pixels is indeterminate to about one or two gray levels and that the gradient of the brightness near cloud edges is small, we do not think it fruitful to make any correction for the above effects.

The area of the kth cloud is simply defined as the number of pixels connected to it multiplied by the area of a single pixel

$$A_k = \sum_{i,j} Q_k(i,j)\Delta x\Delta y \qquad (2)$$

where

$$Q_k(i,j) = 1$$

if the pixel at row i and column j is part of cloud k, otherwise

$$Qk(i,j) = 0.$$

The center of a cloud is defined as its "center of gravity" with respect to brightness, B. Therefore, the mean, brightness-weighted, row coordinate of the center of brightness of the kth cloud is

$$\langle i\rangle_k = \frac{\sum_{i,j} iB_k(i,j)}{\sum_{i,j} B_k(i,j)}. \qquad (3)$$

Similarly, the mean, brightness-weighted, column coordinate of the kth cloud is

$$\langle j\rangle_k = \frac{\sum_{i,j} jB_k(i,j)}{\sum_{i,j} B_k(i,j)}. \qquad (4)$$

The calculation of nearest neighbor spacings (n.n.s.) is based on the assumption that the location of a cloud is defined by its center coordinates. Therefore the nearest neighbor spacing between a cloud, k, and its many neighbors, n, is $(\text{n.n.s.})_k$ where

$$(\text{n.n.s.})_k = \min_n(D_{n,k}) = \min_n[(\langle i\rangle_n - \langle i\rangle_k)^2 + (\langle j\rangle_n - \langle j\rangle_k)^2]. \qquad (5)$$

If any two clouds are isolated and their nearest neighbor spacings identical, they are counted only once in the construction of the histogram. Single clouds less than four pixels in area were not included in the construction of the n.n.s. histograms.

This method of calculation seems justifiable to us as the largest brightness gradients in any given cloud image occur near its maxima of brightness.

3. The distribution of nearest neighbor (n.n.) spacing

The properties of individual clouds such as the size distribution and the fractal dimension of the perimeters are insufficient to specify the two-dimensional morphology of a cloud field. We also need measures for the relation of a cloud to its environment. As we emphasized in section 1, such properties are intimately connected to the physical mechanisms responsible for cloud formation and crucial in computation of the radiative properties of the cloud fields.

When visually analyzing the spacings of clouds in the images, one observes both single clouds and clustered aggregates of single clouds which we define as "cloud clumps"—both in a variety of sizes and separations from each other. The clumps are groups of closely gathered but clearly separated "small" clouds, all of which are smaller than the effective radius at the break in the slope of the size distribution or of the (log perimeter, log area) relationship. Each of the single larger clouds, when analyzed in detail, shows a complex

topographical structure, and one gets the impression that it is composed of a merged clump, or of a closely packed aggregate, of the smaller clouds. All clouds typically show strong brightness gradients close to their single or multiple brightness maxima and the rest of the cloud area is much fainter. Similar results are described elsewhere (e.g., Welch and Wielicki 1986; Wielicki and Welch 1986; Welch et al. 1988).

The "nearest neighbor spacing" (n.n.s.) between cloud brightness centers as defined in Eq. (5) is perhaps the simplest measure of cloud–cloud interaction. Clouds less than four pixels in area are excluded from the analysis because it is difficult to be sure of their proper identification as a separate cloud, especially close to larger clouds. A visual example of the histogram and distribution function of these n.n. spacings is given in Fig. 2 for Band MSS 4 of Case 7025. The results are almost identical to those for the other band analyzed, just as we found for the size distributions and fractal dimensions. The histogram is strongly peaked at a value that varies slightly from scene to scene but is close to 0.5 km. Each data point represents a set of nearest neighbor spacings that have a range equal to the width of the interval between two successive points—a "bin." The width of a bin is about 50 meters; this is narrower on the figure than the diameter of the points. The size of the bin representing a subset of the data was determined by the wish to show the experimental shape of the curve as clearly as possible without blackening the figure with a very large number of points. The standard deviation of the nearest neighbor spacings in each bin is less than the range. We therefore do not show any error bars on our data in the figure. Initially we fitted

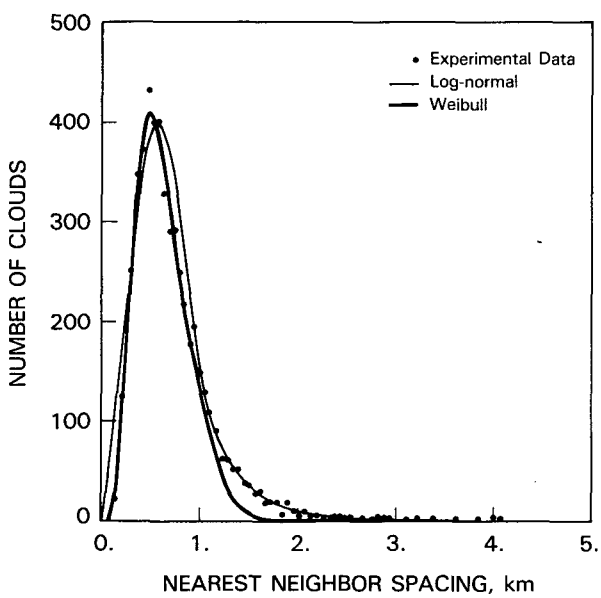

FIG. 2. Histogram and distribution function of nearest neighbor spacing for Case 7025 Band 4. Heavy line: Weibull function fit, thin line- log- normal function fit, +: histogram of experimental data.

our n.n. spacing data to log-normal distributions, as these seemed to be a natural choice due both to the shape of the histograms as well as to the common occurrence of that distribution in many studies of the physical properties of clouds (e.g., Lopez 1977). As may be seen in Fig. 2, the log-normal function fits the data quite well, especially so in the tail of the histogram, for n.n. spacings larger than about one kilometer.

Physically speaking, however, it is difficult to imagine one single atmospheric process that governs the spacing of small boundary layer clouds as well as that of large irregular clouds and cloud clumps. The shape of our size distributions indicates that the formation mechanism leads to the dominance of small clouds in terms of number. The linear dependence of nearest neighbor spacings on effective radii that we find (see the next section) indicates that small clouds tend to be more closely spaced than the larger ones. This agrees with our impression, based on visual inspection of images, that the small clouds often tend to be organized into clumps. Finally, the larger clouds have a significantly larger fractal dimension of the perimeters than the small ones (Cahalan and Joseph 1989), which again points to a different physical formation mechanism. All these facts taken together seem to preclude a single physical formation and areal distribution model. The single lognormal distribution that we can fit to the data on nearest neighbor spacings is therefore likely to be due to the combination of two or more processes, some acting on the smaller clouds and others acting to form and space the large clouds and cloud clumps.

The planar distribution of both clouds and cloud clusters in nonraining fair weather cumulus fields with low-to-medium cloudiness frequently appears to be close to random with independent spacings. As a first trial to find a population rule, we therefore decided to test if the nearest neighbor spacings are consistent with cloud centers that are randomly and independently distributed. This classical problem in statistics dates back to attempts to decide whether telescopic observations of binary stars could be explained by random coincidence. The following analysis is based on the three-dimensional distribution of n.n. spacings derived by Chandrasekhar (1943) from Hertz's work in the last century. We have adapted it to the planar case because the cumulus cloud bases are all at approximately the same height in the atmosphere and there is no chance of spurious nearest neighbors.

Let $W(s)ds$ be the probability that in a system of *independently and identically distributed points in the plane,* the location of the n.n. of any such point is in an annulus $(s, s + ds)$ around it, where s is the distance from the center point. Then $W(s)$ is the product of two probabilites—the probability that there is no point inside the circle of radius s,

$$1 - \int_0^s W(s')ds'$$

and the probability that there is a point anywhere in the annulus $(s, s + ds)$. The latter, under the present assumptions, is proportional simply to the area of the annulus, $2\pi s ds$, and to the average density of points, n, in the plane. The combined probability is thus

$$W(s)ds = \left[1 - \int_0^s W(s')ds'\right] 2\pi n s ds. \quad (6)$$

After manipulation, one gets

$$\frac{d}{ds}\left(\frac{W(s)}{2\pi n s}\right) = -2\pi n s\left(\frac{W(s)}{2\pi n s}\right) \quad (7)$$

which gives directly as a solution

$$W(s) = 2\pi a n s \exp\{-\pi n s^2\} \quad (8)$$

where a is an integration constant, equal to one.

Let us consider for a moment the distribution of the n.n. spacings with respect to azimuth, ϕ, in the plane of the LANDSAT image. The (independent) probability that the randomly oriented vector s lies within the azimuth angle range $[\phi, \phi + d\phi]$ is $d\phi/2\pi$. Since all azimuth angles ϕ of the vector s are equally probable and are independent of s, the azimuth angle dependence integrates out of our problem.

The probability that a n.n. spacing has an amplitude s and lies within the annulus $(s, s + ds)$ centered on one of the cloud centers of brightness in the case of a random distribution of the latters' locations in the plane of the LANDSAT image is thus $W(s)$ as given by Eq. (8). This probability distribution $W(s)$ is a special case, namely $n = 1$, of the Weibull distribution (Walpole and Meyers 1978).

$$W(s) = a s^n \exp[-b(n + 1)], \quad n \geq 0. \quad (9)$$

The Weibull distribution arises if one allows the probability of finding a cloud at a spacing s in the planar annulus not to be independent: in other words, that the conditional probability of finding a cloud at a spacing s from a given cloud depends on s. For example, if the conditional probability is a power law, s^δ, it has been shown (Cahalan 1986) that one again gets a Weibull distribution but with an effective power of

$$n_{\text{eff}} = \delta + 1. \quad (10)$$

where δ is a measure of the deviation from independence $[n_{\text{eff}} = 1]$ of the cloud centers' location in the plane. If δ is negative, there is clumping ("attraction"), if positive, there is "repulsion" between clouds. The Weibull fit is shown on Fig. 2. It agrees well with the n.n. spacing histograms for the spacings less than one kilometer but deviates significantly from the data for the larger spacings.

Integration of Eq. (9) from s to ∞, gives the cumulative probability, W^*, of the n.n. spacing being located between s and ∞, which may be written

$$W^*(s, \infty) \Big/ \left[\frac{a}{b(n_{\text{eff}} + 1)}\right] = \exp(-bs^{(n_{\text{eff}}+1)}).$$

Solving for $\ln(s)$, one gets

$$\ln s = -\frac{\ln b}{n_{\text{eff}} + 1} + \frac{1}{n_{\text{eff}} + 1} \times \ln\left[-\ln\left(\frac{W^*}{a/b(n_{\text{eff}} + 1)}\right)\right] \quad (11)$$

a linear relation with a slope of $(n_{\text{eff}} + 1) - 1$. Plotting the experimental histogram in a form consonant with this function by ranking the data from largest to smallest and normalising by the number of n.n. spacings, makes it possible to check if the n.n. spacings in the plane are random-$n_{\text{eff}} = 1$ (or $\delta = 0$). In that case, we have a slope

$$(n_{\text{eff}} + 1)^{-1} = 0.5. \quad (12a)$$

We have independent attractive clumping, $\delta < 0$, when $n_{\text{eff}} < 1$ or the slope is

$$(n_{\text{eff}} + 1)^{-1} > 0.5; \quad (12b)$$

or repulsion—$\delta > 0$—when

$$(n_{\text{eff}} + 1)^{-1} < 0.5. \quad (12c)$$

The test is applied by observing whether or not the LANDSAT data, plotted in the form of Eq. (11) deviate from a straight line with the slope of 1/2.

We have tested the effectiveness of the above equation to detect a random independent distribution of the locations of cloud centers by applying it to the cloud spacings obtained in a numerical simulation of shallow cumulus convection in the (x, z) plane by VanDelden and Oerlemans (1982). Perturbations on a conditionally unstable lapse rate were inserted at randomly chosen locations along the x-axis. The induced instabilities led to the formation of cumulus clouds at random locations. Our analysis was carried out on the data for the first two hours of the simulation when no organization of the cloud field had as yet taken place. Figure 3a shows that we in fact do get a straight line with a slope of 1/2 indicating an independent distribution of cloud centers. Our results for all LANDSAT 3 cases are given in Table 4 in terms of the parameters of the Weibull fits, a, b and n_{eff}. The parameter a is related to the total number of spacings, b to the width of the distribution. Both n_{eff} and b are again remarkably similar worldwide. This may be due to the occurrence of similar conditions of convection at all locations at the time of measurement—namely, of the midmorning shallow fair weather cumulus type.

The average value and the standard deviation of the power n_{eff} of all the Weibull fits, combining all available data, are 1.07 ± 0.16 and for the parameter b, we have 2.18 ± 0.73. The average peak value, $s_{\max}$, of the histograms is 0.47 ± 0.16 km. The data from the various

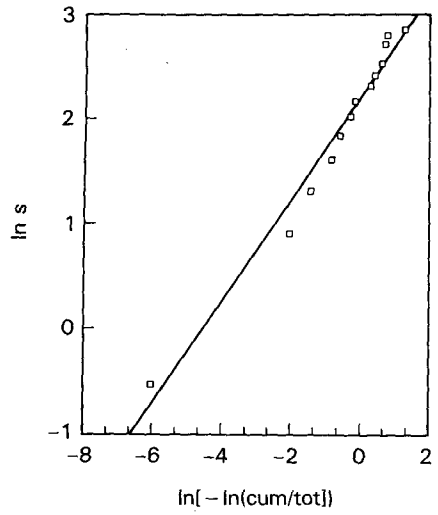

FIG. 3a. Test of the independence of the n.n. spacings between cloud centers applied to the results of a numerical simulation of cloud formation at randomly chosen locations (VanDelden and Oerlemans 1984). The slope of the fit is 0.49—in other words, the power of the Weibull function is 1.04- which means that the distribution of n.n. spacings is independent. The variance of the fit being 0.976, the test for independence of n.n.s. is thus validated.

TABLE 4. Parameters for the Weibull fit to nearest neighbor spacings, averaged over the two bands used, $dN/ds = asn_{\text{eff}} \exp[-bsn_{\text{eff}} + 1]$. For difference between bands see Table 3a; for locations—see Tables 1 or 2b.

Case	n_{eff}	b	a	Noise#
7013	1.53	1.79	222	0.37*
7024	1.27	2.24	471	0.11
7025	1.21	2.37	1453	0.12
7026	1.04	1.66	546	0.08
7028	1.13	1.84	497	0.07
7029	1.33	2.52	942	0.09
7030	1.21	1.08	642	0.17
7033	0.87	1.39	353	0.05
7034	1.11	2.07	230	0.03
7035	0.85	1.82	144	0.04
7036	0.87	1.81	74	0.04
7060	1.26	2.10	1277	0.13
7064	1.09	2.31	519	0.05
7066	1.49	9.10	4300	0.39*
7067	1.00	4.26	719	0.07
7072	1.12	1.82	91	0.02

Noise fraction of cloud pixels.

* Note the high values of the power n_{eff} for the cases with noise above 0.10 percent, especially for the very noisy cases 7013 and 7066. The value of n_{eff} for the quiet case—noise fraction less than 0.10—is 1.04 ± 0.15, indicating behavior close to random.

locations are very similar. Therefore, we show typical examples in Figs. 2 and 3b. It may be seen from these figures that the Weibull function fit to the data is fairly good up to a maximum value of the n.n. spacing of about one kilometer. In order to emphasize this graphically, we present MSS 4 data in Fig. 3b for Case 7024 with an amount of cloudiness of 33.1 percent. Superposed on the experimental data is the Weibull distribution function fitted to them with $n_{\text{eff}} = 1.27 \pm 0.05$ in the form of Eq. (11). The Weibull distribution fits fairly well for n.n. spacings less than about 1 km but increases much less rapidly than the data with increasing n.n. spacing for values of the latter above 1 km. The fact that the slope of the data points for the large clouds is significantly larger than one-half suggests that an "attractive" mechanism is active for these clouds and a Weibull distribution is not useful to describe the data in that size region.

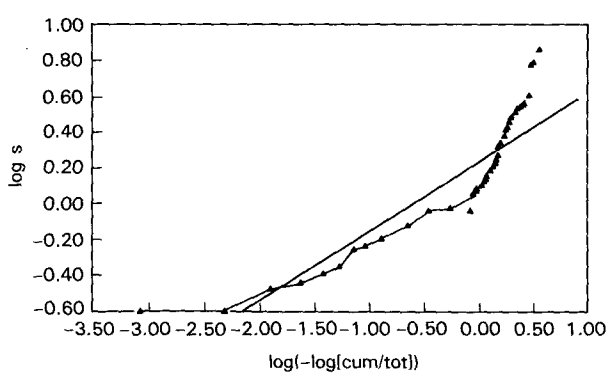

FIG. 3b. Test of the independence of n.n. spacing between cloud centers for bands MSS 4 in case 7024 with a cloud cover of 33.1 percent. The variable s is the nearest neighbor spacing. The independent variable on the Figure is that of Eq. 11 in the text. The power of the Weibull fit is 1.27 ± 0.05 and therefore the slope of the straight line fit to the data is 1/2.27. Note the strong deviation of the data from both the linear fit and from a slope of one-half for n.n. spacings larger than one km.

4. The relationship between effective cloud radius and nearest neighbor spacing

We investigated the relationship between the two basic single cloud parameters described here—the effective radius, r_e, and the n.n. spacing, s, which constitute a unique pair for each cloud. We found that in all cases, the experimental n.n. spacings depend linearly on the effective radii, i.e.,

$$s = Cr_e. \tag{13}$$

The proportionality factor, C, however, varies between 5 and 20 from case to case, without a clear dependence on any other parameter. The linear dependence in each case holds for all values of the effective radius up to and including the largest ones. Figure 4 shows a typical example of these relationships. The fit is very good up to an effective radius of about 500 meters, which is very close to the radius at which the break in the slope

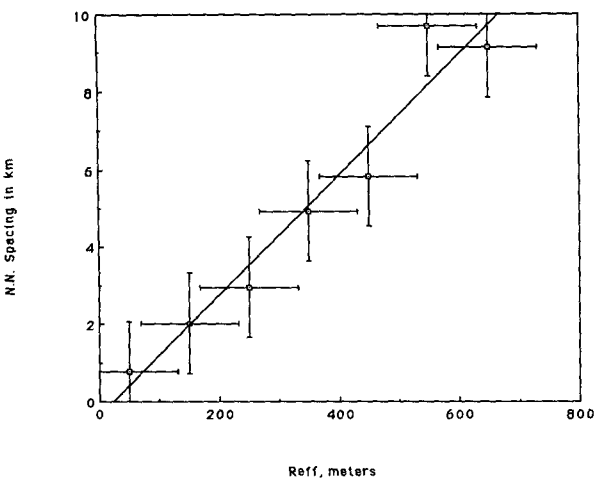

FIG. 4. The linear proportionality of the n.n. spacing and the effective radius—Case 7024. The least squares best fit, with a correlation coefficient of 0.97 is:

$$\text{n.n.s. [km]} = -0.38 + 16 r_{\text{eff}}\,\text{[km]}.$$

of the size distribution occurs in this case—viz. 0.46 km. However, the correlation of the fit using all data, including the large clouds, is still 0.97. Physically, the linear dependence of the n.n. spacing on the effective radius may mean that each individual small shallow nonraining fair weather cumulus cloud forms inside an independent bubble or volume in a horizontally homogenuous atmosphere and interacts only weakly with its neighbors. The upper limit on the horizontal size of the small clouds, presumably formed by boundary layer processes, is determined by the boundary layer thickness since the aspect ratio of nonraining fair weather cumulus clouds in the morning hours is close to one (e.g., Plank 1969; Gagin 1984, private communication). Furthermore, the visible area of such a cloud depends on the amount of water vapor accessible to the convective convergence pattern in which it forms and thus is proportional to the area of its "living space," which we assume to be roughly proportional to πs^2. The linear dependence of the nearest neighbor spacing on the effective cloud radius that we find may reflect this dependence on the available water vapor. The size distribution of the "small" clouds—those between four pixels and the break in the slope of the size and other distributions—is thus determined by the stability, the water vapor content and the dynamical regime in the boundary layer. The upper limit on the horizontal size of the small clouds is probably related to the boundary layer thickness. The large clouds—those larger than the break in the slope of the size and other distributions—should show the same proportionality since they seem to be aggregates of smaller clouds, each, roughly speaking, bringing its own "living space" to the union. The linear relation between n.n. spacing and effective cloud radius is also an indication that the smaller clouds tend to be closer together than the larger ones.

5. Discussion and summary

This study presents the results of an experimental study, using LANDSAT 3 MSS data, of the statistical distribution of nearest neighbor (n.n.) spacings of mid-morning fair weather cumulus cloud fields at 15 locations spread over most of the world's oceans. Obtaining environmental cloud properties like the nearest neighbor spacing is the next step in the description of the complex morphology of cumulus cloud fields beyond the single cloud properties that we and other authors focused on in previous studies. Nonraining fair weather cumulus clouds are typical of large areas of the tropical and subtropical ocean and land areas. Therefore, they are of intrinsic interest in many fields of the atmospheric sciences. The statistical description of these cloud fields will be useful in studies of such topics as shallow moist convection, the radiative balance of the cloudy climate system, the remote sensing of atmospheric and surface properties in the presence of clouds and the parameterization of boundary layer fluxes in climate models.

The interesting common features, reported upon previously (Cahalan and Joseph 1989) of the size distributions and fractal dimensions of fair weather cumulus cloud fields at widely different locations, exist also for the nearest neighbor spacings and for their dependence on the effective radii. Because, nonprecipitating fair weather cumulus clouds usually have aspect ratios of about one from early morning till late afternoon (e.g., Plank 1969; Gagin 1984, private communication), the breaks in the slopes of our experimental cloud radii histograms and the change in the fractal dimension of the perimeters, both at about 500 meters, may have a causal link to the depth of the turbulent boundary layer. A formation mechanism for the small clouds must be consistent with the fractal dimension of their perimeters, which is close to 4/3 (Hentschel and Proccaccia 1984; Cahalan and Joseph 1989).

The effective cloud radii and the associated nearest neighbor spacings are found to be always linearly dependent. This means, in our opinion, that the small fair weather cumulus clouds sampled in our study develop fairly independently of one another and that they tend to be much closer to one another, in comparison with the larger ones.

Testing for independence of the nearest neighbor spacings by fitting their histograms to a Weibull distribution and looking for slopes of 1/2 in diagrams like those in Figs. 2 and 3a, shows that, for n.n. spacings less than about 1 km and associated with clouds having radii less than a few hundred meters, the distribution in the horizontal plane of the centers of clouds is close to independent. For nearest neighbor spacings larger

than 1 km, which are associated with the larger clouds, the actual n.n. spacing histogram falls off significantly more slowly than the Weibull fit with increasing n.n. spacing as shown in Figs. 2 and 3a. This means that in order to explain the clumps of small clouds, the large clouds and the spacings between these two features of the cloud field, one must invoke other mechanisms than random, independent formation. These must include the capability of merging the small clouds in some of the clumps to make a large cloud. The spacings between cloud clumps and large clouds cannot be assumed to be independent of one another. Qualitative corroborative evidence for these conclusions comes also from our visual study of individual brightness maps for the small [$r < r_{break}$] and large [$r > r_{break}$] clouds. These indicate that the smaller clouds—those with the smaller slopes of the size distribution, a smaller fractal dimension, and showing a nearly random and independent spacing of their centers—have only one maximum of brightness, and do frequently appear in clumps. The larger clouds have at least two maxima of brightness, usually look like merged small clouds and have a very complex shape. In summary, the smaller clouds' formation is probably controlled by small-scale turbulence in the boundary layer, that of the larger clouds by mergers of small clouds and other dynamical processes in the free atmosphere.

Further work needs to be done on the morphology of fair weather cumulus cloud fields. Discrimination techniques could be applied to parameters such as cloud perimeters, area and spacing to objectively separate the size classes. It would be very interesting to extend the availability of LANDSAT-type data to other times of day in order to study the time variation of the Cumulus cloud field parameters (e.g., see Plank 1969). In addition, it is important to extend the lower limit of resolution of the LANDSAT data in order to ascertain the behavior of very small clouds. These aims might be attained by analysis of imagery from other similar satellites or from aircraft-based instrumentation. Another important topic for climate modeling will be to determine relationships between satellite-estimated cloud brightness, in situ measurements of cloud liquid water and the water vapor field.

Acknowledgments. The able scientific programming efforts of Mrs. S. Rechavi, Mrs. Z. Rosen and Mrs. S. Adler were a major factor in the success of this study. We are much obliged for relevant discussions to Professors B. Gelchinski and Y. Mekler as well as to Drs. V. Kagan, R. Kahn and D. Starr. Short collaborations with Drs. R. Kahn and V. Kagan are gratefully acknowledged. This study was funded in part by US Air Force Grants AFOSR-83-0239, AFOSR-86-0174 and by BSF Grant 3089/82 of the US–Israel Bi-National Science Foundation. The final part of this research was carried out while one of us [JHJ] held an NRC Senior Research Associateship at the Goddard Space Flight Center.

REFERENCES

Baker, M., and J. Latham, 1979: The evolution of droplets and the rate of production of embryonic raindrops in small cumulus clouds. *J. Atmos. Sci.*, **36**, 1612–1615.

Betts, A. K., and M. J. Miller, 1986: A new convective adjustment scheme, II-Single column tests using GATE wave, BOMEX and arctic air-mass data sets. *Quart. J. Roy. Meteor. Soc.*, **112**, 693-710.

Blackmer, R. H., and S. M. Serebreny, 1962: Dimensions and distributions of cumulus clouds as shown by U-2 photographs, Rep. No. 62-609, S.R.I., AFCRL, 57 pp.

Bretherton, C. S., 1987a: A theory of non-precipitating moist convection between two parallel plates. Part 1: Thermodynamics and linear solutions. *J. Atmos. Sci.*, **44**, 1809–1827.

——, 1987b: Linear propagating non-precipitating moist convection. *J. Atmos. Sci.*, **44**, 1869–1874.

Cahalan, R. F., 1986: Nearest neighbor spacing distributions of cumulus clouds. *Proc. of the Second Int. Conf. on Statistical Climatology*, Vienna.

——, 1989: Overview of fractal clouds. RSRM87: *Advances in Remote Sensing*, A. Deepak, 371–388.

——, and J. H. Joseph, 1989: Fractal statistics of cloud fields. *Mon. Wea. Rev.*, **117**, 261–272.

——, and J. B. Snider, 1989: Stratocumulus structure. *Remote Sens. Environ.*, **27**, 95–107.

——, D. A. Short and G. R. North, 1981: Cloud fluctuation statistics. *Mon. Wea. Rev.*, **110**, 26–43.

Chandrasekhar, S., 1943: Stochastic problems in physics and astronomy. *Rev. Modern Phys.*, **15**, 1–89.

Cho, H. R., 1978: Some statistical properties of a homogenuous and stationary shallow cumulus field. *J. Atmos. Sci.*, **35**, 125–138.

Clark, T. W., T. Hauf and J. P. Kuettner, 1986: Convectively forced internal gravity waves: Results from two-dimensional numerical experiments. *Quart. J. Roy. Meteor. Soc.*, **112**, 899–925.

Davies, R., 1978: The effect of finite geometry on the three-dimensional transfer of solar radiation in clouds. *J. Atmos. Sci.*, **35**, 1712–1725.

Derr, V., and R. Gunter, 1982: EPOCS 1980: Summary data report—Aircraft measurements of radiation, turbulent transport and profiles in the atmospheric and oceanic boundary layers of the tropical Eastern Pacific, NOAA Tech. Memo. ERL WPL-101, Wave Propagation Lab., Boulder.

Fraedrich, K., 1976: A mass budget of an ensemble of transient cumulus clouds determined from direct cloud observations. *J. Atmos. Sci.*, **33**, 262–268.

——, 1977: Further studies on a transient cumulus cloud ensemble and its large scale interaction. *J. Atmos. Sci.*, **34**, 335–343.

Gube, M., J. Schmetz and E. Raschke, 1980: Solar radiative transfer in a cloud field. *Contrib. Atmos. Phys.*, **53**, 24–34.

Hahn, C. J., S. G. Warren, J. London, R. Chervin and R. Jenne, 1984: Atlas of simultaneous occurrence of different cloud types over land. NCAR/TN-241-STR, 21 pp.

Harshvardan, and R. W. L. Thomas, 1984: Solar reflection from interacting and shadowing cloud elements. *J. Geophys. Res.*, **89**, 7179–7185.

Hentschel, H. G. E., and I. Proccaccia, 1984: Relative diffusion in turbulent media, the fractal dimension of clouds. *Phys. Rev.*, **A29**, 1461–1476.

Hozumi, K., T. Harimaya and C. Moano, 1982: The size distribution of cumulus clouds as a function of cloud amount. *J. Meteor. Soc. Japan*, **60**, 691–699.

Joseph, J. H., 1985: The role of cloud field morphology in weather and climate studies, *Isr. J. Earth Sci.*, **34**, 96–101.

——, 1986: The study of cloud morphology from LANDSAT, Final Report Air Force Grant AFOSR-83-0239, 137 pp.

——, 1987: The study of Cumulus cloud field morphology from LANDSAT 4, Final Report Air Force Grant AFOSR 86-0174, 26 pp.

——, and V. Kagan, 1988: The reflection of solar radiation from bar cloud arrays. *J. Geophys. Res.*, **93,** 2405–2417.

Kaufman, Y. J., 1987: The effect of sub-pixel cloud formation on remote sensing. *Int. J. Remote Sensing,* **8,** 839–857.

Lopez, R. E., 1977: The log-normal distribution and cumulus cloud populations, *Mon. Wea. Rev.*, **105,** 865–872.

Lovejoy, S., 1982: Area-perimeter relation for rain and cloud areas, *Science,* **216,** 185–187.

Mandelbrot, B., 1984: *The Fractal Geometry of Nature,* Freeman, 461 pp.

Paltridge, G. W., 1974(a): Atmospheric radiation and the gross character of stratiform clouds, *J. Atmos. Sci.*, **31,** 244–250.

——, 1974(b): Global cloud cover and Earth surface temperature. *J. Atmos. Sci.*, **31,** 1571–1576.

Plank, G. W., 1969: The size distribution of cumulus clouds in representative Florida populations. *J. Appl. Meteor.*, **8,** 46–67.

Randall, D., and A. Huffman, 1980: A stochastic model of cumulus clumping, *J. Atmos. Sci.*, **37,** 2068–2078.

Stephens, G. L., 1976: The transfer of radiation through vertically non-uniform stratocumulus clouds. *Contrib. Phys. Atmos.*, **49,** 237–253.

Simpson, J., N. Westcott, R. Clarman and R. A. Pielke, 1980: !On Cumulus mergers. *Archiv. Met. Bioklim., Ser. A,* **29,** 1–40.

VanDelden, A., and J. Oerlemans, 1982: Grouping of clouds in a numerical cumulus convection model. *Beitr. Phys. Atmos.*, **55,** 239–252.

Walpole, R. E., and R. H. Myers, 1978: *Probability and Statistics for Engineers and Scientists,* 2 ed., Macmillan, 580 pp.

Welch, R. M., and B. A. Wielicki, 1985: A radiative parameterisation of stratocumulus cloud fields, *J. Atmos. Sci.*, **42,** 2888–2897.

——, S. K. Cox and I. M. Davies, 1980: *Solar Radiation and Clouds, Met. Monog.,* Amer. Meteor. Soc., **17,** 96 pp.

——, K. S. Kuo, B. A. Wielicki, S. K. Sengupta, and L. Parker, 1988: Marine stratocumulus cloud fields off the coast of Southern California observed using LANDSAT imagery. Part I: Structural characteristics. *J. Appl. Meteor.*, **27,** 341–362.

Wielicki, B. A., and R. M. Welch, 1986: Cumulus cloud properties derived using LANDSAT satellite data. *J. Climate Appl. Meteor.*, **25,** 261–276.